Bull. Chem. Soc. Ethiop. **2025**, 39(4), 659-672.
DOI: https://dx.doi.org/10.4314/bcse.v39i4.5
© 2025 Chemical Society of Ethiopia and The Authors
ISSN 1011-3924
Printed in Ethiopia
Online ISSN 1726-801X

NEW OXOMOLYBDENUM(IV) COMPLEXES WITH ADDUCTED MONODENTATE LIGANDS, SPECTROSCOPIC CHARACTERIZATION, DFT CALCULATIONS, BIOLOGICAL AND ANTIOXIDANT ACTIVITY

Noor F. Abdalah[1,3], Othman I. Alajrawy[2] and Sattar R. Majeed[3]

[1]Higher Health Institute, Ramadi, Anbar, Iraq
[2]Department of Biology, College of Education, University of Fallujah, Iraq
[3]Department of Chemistry, College of Science, Anbar University, Iraq

(Received July 26, 2024; Revised December 29, 2024; Accepted January 3, 2025)

ABSTRACT. Oxomolybdenum(IV) complexes with chemical formula [MoO(ATP)(DIAB)(AMP)] (C1), [MoO(ATP)(DIAB)(Atri)] (C2), [MoO(ATP)(HNQ)(AMP)] (C3) and [MoO(ATP)(HNQ)(Atri)] (C4) have been synthesized and studied using different spectral methods, including atomic absorption, FTIR, UV-Vis., mass spectroscopy, magnetic sensitivity, electrical conductivity, and C.H.N.S. analysis. The ligands were 2-aminothiophenol (ATP), 3,4-diaminobenzoic acid (DIAB), 2-hydroxy-1,4-naphthoquinone (HNQ), 6-amino-2-methylpyridin (AMP), and 3-amino-1,2,4-triazole (Atri). The FTIR spectra confirm (DIAB, AMP, and Atri) were coordinated by amine nitrogen, whereas the (HNQ) ligand was by oxygen, and the (ATP) by nitrogen and sulfur atoms. The υ(S-H) band vanished in comparison to the (ATP) ligand, this demonstrates how Mo(IV) and the sulfur atom. The (HNQ) ligand's oxygen atoms work in tandem with the Mo(IV). Mo(IV) complexes with d^2 are paramagnetic. All complexes have been suggested to have an octahedral structure based on computed and experimental evidences. Two Gram-positive and two Gram-negative bacteria were used to test the (ATP) ligand and the produced complexes' activity. The complexes showed an expanded zone of inhibition, indicating that they were more lipophilic than the free (ATP) ligand. Finally, the antioxidant activity of the complexes was tested, and the result showed the following order: Gallic acid > C3 > C2 > C4 > C1 in 60 min.

KEY WORDS: Oxomolybdenum(IV) complexes, 2-Aminothiophenol, 3,4-Diaminobenzoic acid, 2-Hydroxy-1,4-naphthoquinone, 6-Amino-2-methylpyridine, Antioxidant activity

INTRODUCTION

The synthesis of novel, useful complexes from relatively simple chemical molecules relies heavily on transition metal complexes [1]. Because of its several stable and accessible oxidation states and its flexible coordination chemistry, molybdenum is involved in numerous biological and commercial activities [2]. Oxidation states for molybdenum range from (II) to (VI), with the oxidation states from (II-V) being air-sensitive [3]. Molybdenum chemistry is highly fascinating because it can be found in a wide variety of oxidation states, and it can also be found in stable complexes with ligands that include oxygen, nitrogen, and sulfur atoms. These ligands may have a wide range of coordination numbers and stereo chemistry. The amount of oxy-groups that are connected to molybdenum in oxo-complexes determines its oxidation state. The two terminal oxygen atoms can frequently be observed in Mo(VI) and (V) ion-formed cis- or trans-dioxo complexes [4]. $[cis\text{-}MoO_2]^+$ complexes are the most prevalent, they contribute to a wider range of organic changes. This is because MoO_2(VI) compounds are very simple to synthesize and have simple chemical properties. Several MoO_2(VI) complexes, including $[MoO_2(acac)_2]$ and $[MoO_2Cl_2]$, have been utilized to ascertain the form of the remaining anionic ligands [5, 6]. Research revealed that catalysts based on active transition metal centers, like Mo, demonstrated a high level of reactivity when using oxygen and hydrogen peroxide, which are oxidizing agents that are less harmful to the environment [7]. Molybdenum complexes have drawn a lot of attention

*Corresponding authors. E-mail: othman_ibraheem2000@yahoo.com
This work is licensed under the Creative Commons Attribution 4.0 International License

in the fields of biochemistry, catalysis, and medicine because it is known that over fifty enzymes in each kingdom of life depend on molybdenum, making it an essential element required in most biological systems [8], preventive of dental cavities [9], treatment of anemia, enhancement of immunological responses, and antibacterial, antidiabetic, and anticancer medicine [10, 11]. Molybdenum can be reduced to a lower oxidation state (III, IV, and V) during synthesis if a reducing agent is applied [12]. Recent years have seen a surge in interest in molybdenum's coordination chemistry in its (IV) oxidation state as scientists have come to understand that this element is a crucial trace element in a wide range of redox enzymes [13]. Iker Berasaluce *et al.* [14] prepared molybdenum(IV) complexes with a variety of ligands, which act as antidiabetic and anticancer agents. Mina *et al.* [15] also prepared a Mo(IV) complex with LSQ (2,4-dibutylsimibenzoquinone ligand) with the chemical formula [$MoOL^{BIS}L^{SQ}$] as a catalyst for the selective oxidation of sulfides and the oxidative cleavage of cyclohexene.

Octahedral molybdenum cluster complexes have emerged in recent years as singlet oxygen photo-sensitizers with potential uses in biology [16]. Furthermore, a wide range of applications in the domains of energy conversion and storage are made feasible by the numerous structural variants of MoO_x. Molybdenum compounds have been used extensively in analytical chemistry for colorimetric testing. The colorless 2-aminothiophenol (ATP) ligand is soluble in organic solvents as well as water. ATP is a helpful reagent in the field of synthetic chemistry in addition to being a bifunctional organic chemical [17]. ATP is one of the many molecules of interest in medicinal chemistry because of its numerous biological actions, such as its resistance to infections, and, cancer [18]. DIAB ligand is an aromatic amine with effective diamine groups that functions as a bidentate ligand. According to recent studies, DIAB might be a useful tool for creating aminopeptidase inhibitors that are specific to a certain class. One of the naturally occurring 1,4-naphtha-quinone molecules is (HNQ) [19]. A naturally occurring bidentate ligand is (HNQ) [20]. HNQ metal complexes have been demonstrated to be very cytotoxic to cancer cells [21].

EXPERIMENTAL

Materials

We purchased the following from Aldrich: AMP ligand (C6H8N2), Atri ligand (C2H4N4), DIAB ligand ($C_7H_8N_2O_2$), HNQ ligand ($C_{10}H_6O_3$), ATP ligand ($NH_2C_6H_4SH$), and ammonium molybdate(VI) $(NH_4)_2MoO_4$. Solvents of analytical grade were used. $[MoO_2(acac)_2]$ was the first complex to be synthesized, following the guidelines provided in the published research [22].

Instrumentation

In a quartz cell with a 1.0 cm path length, a Shimadzu UV-Visible spectrophotometer recorded the UV-Vis. spectra in 1×10^{-3} M DMSO solution between 200 and 1100 nm. FT-IR measurements were conducted with a Bruker Tensor 27 FT-IR spectrophotometer within the 4000-400 cm^{-1} range. Model EA 3000 single V Eurovector.3. A single elemental microanalysis that is documented (C.H.N. and S.). Using a Shimadzu MSQP50A (E170 eV), mass spectrometry was performed. The magnetic susceptibility was measured using the Balance Magnetic Susceptibility Model (MSBMKI). Molar conductivity was measured with the WTW Xylem digital conductivity meter. Atomic absorption in flames was measured with a Shimadzu AA680 spectrophotometer.

Preparation of the complexes

Preparation of the $[MoO_2(acac)_2]$ complex

The synthesis of $[MoO_2(acac)_2]$ was carried out following the published research [22]. After dissolving (5 mmol, 1 g) of $(NH_4)_2MoO_4$ in 25 mL of distilled water, the solution of (acac) ligand

2 mL was added dropwise. Hydrochloric acid (6 N) was then added to the mixture until the pH reached to 1. The product was repeatedly cleaned in cold water following the filtering process, and the following day it was dried in a desiccator. It was discovered after collection that it was a yellow solid.

Preparation of the C1 complex

$[MoO_2(acac)_2]$ (1 mmol, 0.328 g) was dissolved in 5 mL of absolute ethanol. Next, the ATP ligand solution (1 mmol, 0.125 g) was gradually added to 10 mL of absolute ethanol. After that, three drops of triethylamine (TEA) were added. After an hour, the DIAB ligand (1 mmol, 0.152 g) was dissolved in 20 mL of absolute ethanol. After two hours of reflux, the triphenylphosphine solution (1 mmol, 0.262 g) was added and refluxed for two hours. Finally, 10 mL of 100% ethanol was added to a solution containing (1 mmol or 0.108 g) of the AMP ligand. For two hours, the mixture was refluxed. Filtered, repeatedly cleaned with 100% ethanol, and allowed to dry for 24 hours in a desiccator. 63% of the yield, m.p. = 330-332 °C. Scheme 1 as represented example for the prepared complexes.

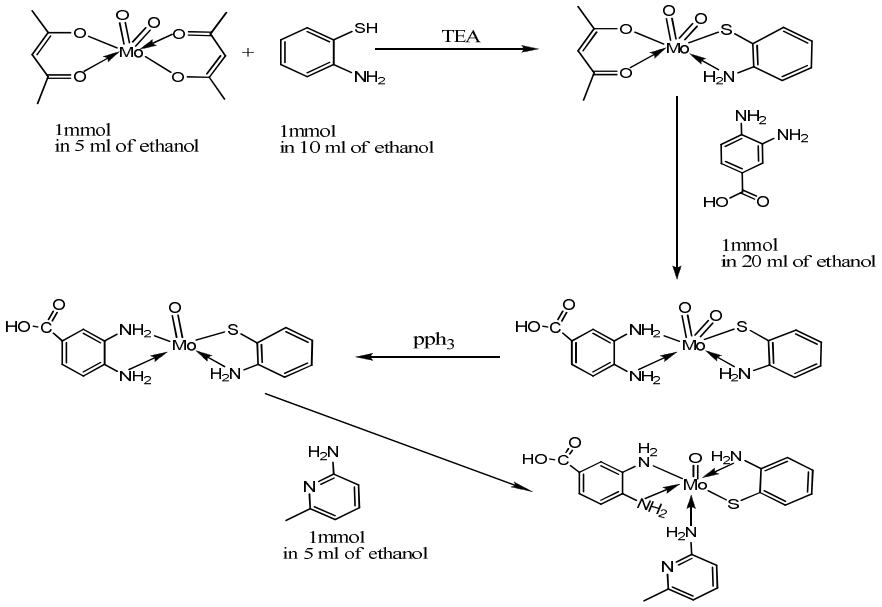

Scheme 1. The preparation reaction for the C1 complex.

Preparation of the C2 complex

The first step involved dissolving of $[MoO_2(acac)_2]$ (1 mmol, 0.328 g) in 5 mL of absolute ethanol. Next, the ATP ligand (1 mmol, 0.125 g) was gradually added to 10 mL of absolute ethanol. Next, three drops of TEA were added. The DIAB ligand (1 mmol, 0.152 g) was dissolved in 20 mL of absolute ethanol. Then, triphenylphosphine solution (1 mmol, 0.262 g) was added. Finally, the (Atri) ligand dissolved in 10 mL of absolute ethanol (1 mmol, 0.084 g) was added. For two hours, the mixture was refluxed. Filtered, repeatedly rinsed with pure ethanol, and dried for a whole day in a desiccator. 65% yield, m.p. = 334-336 °C.

Preparation of the C3 complex

The $[MoO_2(acac)_2]$ (1 mmol, 0.328 g) dissolved in 5 mL of absolute ethanol. (1 mmol 0.125 g) of ATP ligand was dissolved in 5 mL of absolute ethanol. Next, HNQ ligand (1 mmol, 0.174 g) was dissolved in 20 mL of absolute ethanol. Three drops of TEA were added. Then, triphenylphosphine solution (1 mmol 0.262 g) dissolved in 10 ml of absolute ethanol was added. Finally, the AMP ligand dissolved in 10 mL of 100% ethanol (1 mmol, 0.108 g) was added, and for two hours, the mixture was refluxed. Filtered, repeatedly rinsed with pure ethanol, and dried for a whole day in a desiccator. 65% yield, m.p. = 325-328 ºC.

Preparation of the C4 complex

$[MoO_2(acac)_2]$ (1 mmol, 0.328 g) dissolved in 5 mL of absolute ethanol, then the ATP ligand (1 mmol, 0.125 g) dissolved in 10 mL of absolute ethanol was gradually added, then three drops of the TEA was added, then the (HNQ) ligand (1 mmol, 0.174 g) dissolved in 20 mL of absolute ethanol, and triphenylphosphine solution (1 mmol, 0.262 g) dissolved in 10 mL of absolute ethanol was added. Finally, (1 mmol, 0.084 g) of the (Atri) ligand dissolved in 10 mL of absolute ethanol was added. The mixture refluxed for two hours. Filtered, washed many times with absolute ethanol, and then dried in a desiccator for 24 h 68% Yield, m.p. = 312-314 ºC.

Biological activity

Antibacterial activity

Diffusion in holes was used to test the ATP ligand and the complexes against the bacteria *Acinetobacter baumannii (A. baumannii)*, *Escherichia coli (E. coli)*, *Bacillus licheniformis (B. licheniformis)*, and *Staphylococcus aureus (S. aureus)* to ascertain their antibacterial activity. Using a sterile cotton swab, the activated bacterial isolates were evenly distributed throughout the surface of the dish. Give the dishes fifteen to twenty minutes at room temperature to soak and dry. The plates were punctured using a cork punch, and forty microliters of the ligand and the complexes were dissolved in 1 mL of the DMSO. The ligand and the complexes concentrations were 100, 50, 25, and 12.5 ppm, respectively. DMSO was the control factor that was employed; it has no inhibitory effect. According to the reference, the experiment comprised measuring the millimeter-circumference of the growth inhibition zones and incubating the plates at 37 ºC for 24 hours.

Minimum inhibitory concentration

The minimum inhibitory concentration (MIC) of antibiotics was calculated using the culture broth microdilution technique [23]. The models were incubated at 35-37 ºC for 24 hours in the incubator. Using ELISA equipment, the MIC test findings were interpreted because solutions with high turbidity often have high absorbance. The intended outcome was obtained by comparing the blank's processing absorption and measuring the turbidity (growth). The MIC exhibits the least amount of microbial growth suppression.

Antioxidant activity by DPPH (2,2-diphenyl-1-picrylhydrazyl)

1. Various concentrations of each sample were combined with 100 µL. Four concentrations were employed in each sample, and they varied based on the concentrations of each chemical. 2. The reaction takes happen for 60 min at room temperature in a dark area. 3. The hue changes from dark violet to bright yellow as the produced antioxidant complexes react with DPPH.

4. The absorbance at 517 nm wavelength was determined by UV-Visible spectroscopy. 5. Determine the root scavenging %. 6. The produced compounds were compared to gallic acid as a reference to see how well they suppressed free radicals.

RESULTS AND DISCUSSION

The synthesized complexes were examined using elemental microscopic analysis and the atomic absorption method to ascertain the molybdenum content of the complexes. As seen in Table 1, the experimental (C.H.N.S.) findings were consistent with the theory underlying the suggested formulation of the complexes.

Table 1. The elemental analysis (C.H.N.S.) for the complexes.

Complexes	Calc. Exp.	Elemental analysis				
		C%	H%	N%	S%	M%
C1	Calc.	46.06	4.27	14.14	6.47	19.37
	Exp.	47.01	4.87	15.11	5.49	20.12
C2	Calc.	38.22	3.64	20.80	6.80	20.35
	Exp.	39.12	4.22	19.97	5.89	21.28
C3	Calc.	51.07	3.70	8.12	6.20	18.54
	Exp.	50.45	4.12	7.86	7.11	19.48
C4	Calc.	43.82	3.06	14.20	6.50	19.45
	Exp.	42.89	3.94	13.82	7.23	20.19

FT-IR spectra

The FT-IR spectra for the compounds are displayed in Table 2. The C1 and C2 complexes' spectra showed bands at 3417 and 3347 cm^{-1} and 3417 and 3347 cm^{-1}, respectively, which corresponded to the amine group's symmetrical and asymmetrical stretching vibrations DIAB, ATP, AMP, and Atri ligands, these bands were transferred to different frequencies. This demonstrates how the nitrogen atoms coordinate the ligands in the C1 and C2 complexes with the Mo(IV) ion. In the prepared complexes, the υ(S-H) bands vanished in contrast to the ATP ligand. This demonstrates that the sulfur atom facilitates the coordination of the ATP ligand. The stretching of υ(NH), υ(M=O), υ(M-S), and υ(M-N) correspond to the appearance of new extra bands at 3281, 902, 660, and 459 cm^{-1} in the C1 complex and 3281, 902, 667, and 464 cm^{-1} in the C2 complex, as seen in Figure 1 for the complex C1 as represented for the complexes, in that order. The C3 and C4 complexes' spectra revealed bands at 3409 and 3324 cm^{-1} and 3348 and 3285 cm^{-1}, respectively, which corresponded to the amine group's symmetrical and asymmetrical stretching frequencies. When compared to the free ligands, these bands were shifted to different frequencies. This demonstrates how the nitrogen atoms that make up the amine group coordinate the ATP and AMP ligands in the C3 complex and the ATP and Atri ligands in the C4 complex with the Mo(IV) ion. In C3 and C4 complexes, υ(S-H) bands vanished in contrast to the ATP ligand. This data demonstrates that the coordination of the Mo(IV) ion with the ATP ligand is caused by the sulfur atom. In the generated complexes, the υ(OH) bands disappeared in contrast to the HNQ ligand. The coordination between the Mo(IV) ion and the HNQ ligand is established through the oxygen atoms in the hydroxyl group. The stretching of υ(M=O), υ(M-O), and ν(M-N) is responsible for the appearance of new bands at 926, 551, and 456 cm^{-1} in the C3 complex and 926, 561, and 463 cm^{-1} in the C4 complex, respectively [24]. The estimated data of optimal compounds generated from the DFT calculation using the G 09W software were compared with the experimental FTIR data of the MoO(IV) complexes, and they agreed well with the experimental ones. The various techniques utilized to collect each data point account for the discrepancies between the computed and experimental results.

Table 2. FTIR bands experimental and calculated of the ligands and prepared the complexes.

Compound	Exp.	Calc.	Assignment
ATP	3377, 3296	3541, 3365	νNH_2
	1566	1636	δNH_2
	2643	2641	νS-H
DIAB	3420	3561	νOH
	3329, 3207	3462, 3357	νNH_2
	1544	1633	δNH_2
	1623	1682	νC=O
HNQ	3465	3583	νOH
	1679	1740	νC=O
AMP	3460, 3316	3581, 3455	νNH_2
	1599	1630	δNH_2
Atri	3412, 3332	3581, 3477	νNH_2
	1593	1660	δNH_2
C1	3417, 3347	3435, 3500	νNH_2
	1642	1680	δNH_2
	902	977	M=O
	660	700	M-S
	459	550	M-N
C2	3417,3347	3422, 3488	νNH_2
	1543	1622	δNH_2
	902	984	M=O
	667	710	M-S
	464	523	M-N
C3	3409,3324	3495, 3574	νNH_2
	1642	1691	δNH_2
	926	1000	M=O
	551	620	M-O
	456	546	M-N
C4	3348,3285	3498, 3318	νNH_2
	1543	1614	δNH_2
	926	1000	M=O
	561	634	M-O
	463	541	M-N

Mass spectral analysis

The mass spectroscopic data for the complexes are measured, the molecular ion (M) peak of the C1 complex (M.Wt. = 495.41) is located at m/z = 494.40, the ($C_{18}H_{19}MoN_5OS^+$) peak is located at m/z = 449.38, the ($C_{12}H_{12}MoN_3OS^+$) peak is located at m/z = 342.25, the ($C_{12}H_{11}MoN_2OS^+$) peak is located at m/z = 327.23, the ($C_6H_6MoNOS^+$) peak is located at m/z = 236.12, the ($C_6H_7MoN_2^+$) peak is located at m/z = 107.13, and the ($C_6H_6N^+$) peak is located at m/z = 92.12. The molecular ion (M) peak of the C2 complex (M.Wt. = 471.35) was followed by the ($C_{13}H_{14}MoN_4O_3S^+$) peak at m/z = 402.15, the ($H_3MoN_2O^+$) peak at m/z = 142.61, the ($C_7H_6NO_2^+$) peak at m/z = 136.21, and the ($C_6H_6NS^+$) peak at m/z = 124.45. The molecular ion (M) peak of the C3 complex (M.Wt. = 517.41) was at m/z = 517.64, the ($C_{11}H_6MoN_3OS^+$) peak was at m/z = 324.19, the ($C_6H_2MoNOS^+$) peak was at m/z = 232.51, the ($C_{10}H_4O_2^+$) peak was at m/z = 156.22, and the ($C_5H_5N_2^+$) peak was at m/z = 93.42. The molecular ion (M) peak of the C4 complex (M.wt = 493.45) was at m/z = 492.35, followed by the ($C_{16}H_{12}MoN_2O_4S^+$) peak at m/z = 424.28, the ($C_{16}H_{11}MoNO_4S^+$) peak at m/z = 409.27, the ($C_{16}H_{10}MoO_4S^+$) peak at m/z = 394.25, the ($C_{10}H_5MoO_4^+$) peak at m/z = 285.08, the ($C_{10}H_6O_2^+$) peak at m/z = 158.15, and the (MoO^{2+}) peak

at m/z = 127.94. The molecular weights of the complexes in the suggested formula are supported by these results.

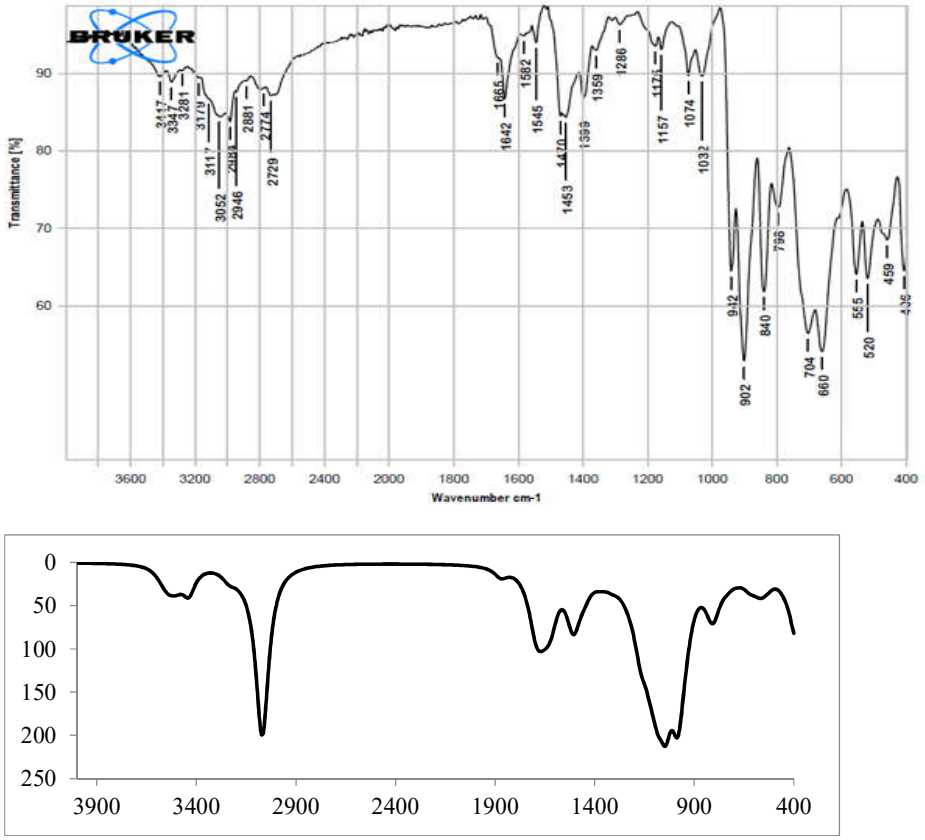

Figure 1. The experimental (up) and calculated (down) FTIR spectra of the C1 complex.

Electronic spectra

For the complexes dissolved in DMSO solutions, electronic spectra were collected at 200–1100 nm. The (π-π*) transition is linked to the absorption peak of the C1 complex, which is located at a wavelength of 270 nm. Moreover, two peaks are attributed to the (n-π*) transition with wavelengths of 308 and 330 nm. As seen in Fig. 2, the absorption spectrum also reveal two peaks for the d-d transition for the complex $^3T_1g(F)\rightarrow{}^3T_2g(F)$ and $^3T_1g(F)\rightarrow{}^3T_1g(p)$; at 609 nm and 817 nm, respectively. The C2 complex contains two peaks at 692 and 988 nm for d-d transition assigned to $^3T_1g(F)\rightarrow{}^3T_2g(F)$ and $^3T_1g(F)\rightarrow{}^3T_2g(p)$; respectively, and an absorption peak at 282 nm assigned to (π-π*) transition, a peak at wavelengths 338 allocated to (n-π*) transition. The C3 complex exhibits two peaks at 560 nm and 912 nm for d-d transition ascribed to $^3T_1g(F)\rightarrow{}^3T_2g(F)$ and $^3T_1g(F)\rightarrow{}^3T_1g(p)$; respectively, and absorption peaks at 262 nm and 307 nm which are attributed to (π-π*) and (n-π*) transition, respectively. The absorption peak locations of the C4 complex: 245 nm is ascribed to the (π-π*) transition, 285 nm to the (n-π*) transition, and 542 nm to the $^3T_1g(F)\rightarrow{}^3T_2g(F)$ [25].

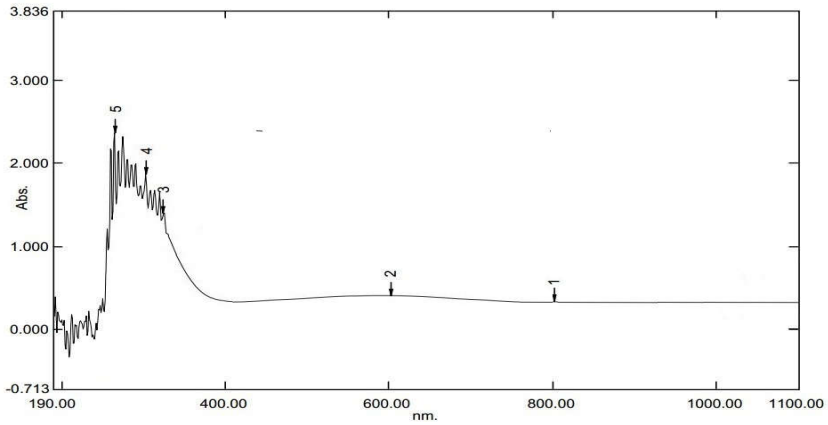

Figure 3. The experimental UV-Vis. spectrum of the C1 complex.

Magnetic susceptibility measurements

All of the complexes exhibited the paramagnetic d^2 electronic configuration (t_2g^2, eg^0) throughout the magnetic susceptibility experiments. For every complex, the range of efficient magnetic moments (μ_{eff}) was between 2.00 and 2.51 [26].

Theoretical studies

The structures of the ligands and the complexes were optimized using different basis sets: the B3LYP/6-31G(d,p) for the ligands and the B3LYP/LanL2DZ for the complexes [27-29]. The proposed structures of the complexes with natural bond order (NBO) charges are shown in Figure 4. When compared to the Mo(IV) complexes that have been reported, the angles around the Mo(IV) atoms in the four complexes match the published values [26, 30]. The divergence of these angles from the optimal value of (90º) for octahedral structures supports the deformed octahedral structures for the complexes. The range of Mo-S bond lengths is (2.39-2.44 Å). The expected donor properties and the ligands' binding sites are supported by their higher charge concentrations on the nitrogen and sulfur atoms [31]. The positively charged Mo(VI) atoms are the acceptors. The electrical energy, atomic charges, and dipole moments for the complexes and ligands are shown in Table 3.

Table 3. The calculated quantum chemical parameters of the ligands and the Mo(IV)complexes by DFT/B3LYP/6-31G(d, P) for the ligands and LanL2DZ for the complexes basis sets.

Compound	HOMO a.u.	LUMO a.u.	η	ΔE a.u.	Electronic energy a.u.	D.M. Debye
ATP	-0.205	-0.006	0.099	0.199	-685.80	1.76
DIAB	-0.208	-0.036	0.086	0.172	-531.68	3.96
HNQ	-0.257	-0.116	0.070	0.141	-610.35	3.02
AMPY	-0.206	-0.008	0.099	0.198	-342.98	1.57
ATri	-0.213	-0.017	0.098	0.196	-297.61	2.04
C1	-0.308	-0.255	0.026	0.053	-1122.87	7.30
C2	-0.304	-0.178	0.063	0.126	-1080.22	9.69
C3	-0.197	-0.136	0.030	0.061	-1392.55	5.20
C4	-0.198	-0.137	0.030	0.061	-1347.19	4.71

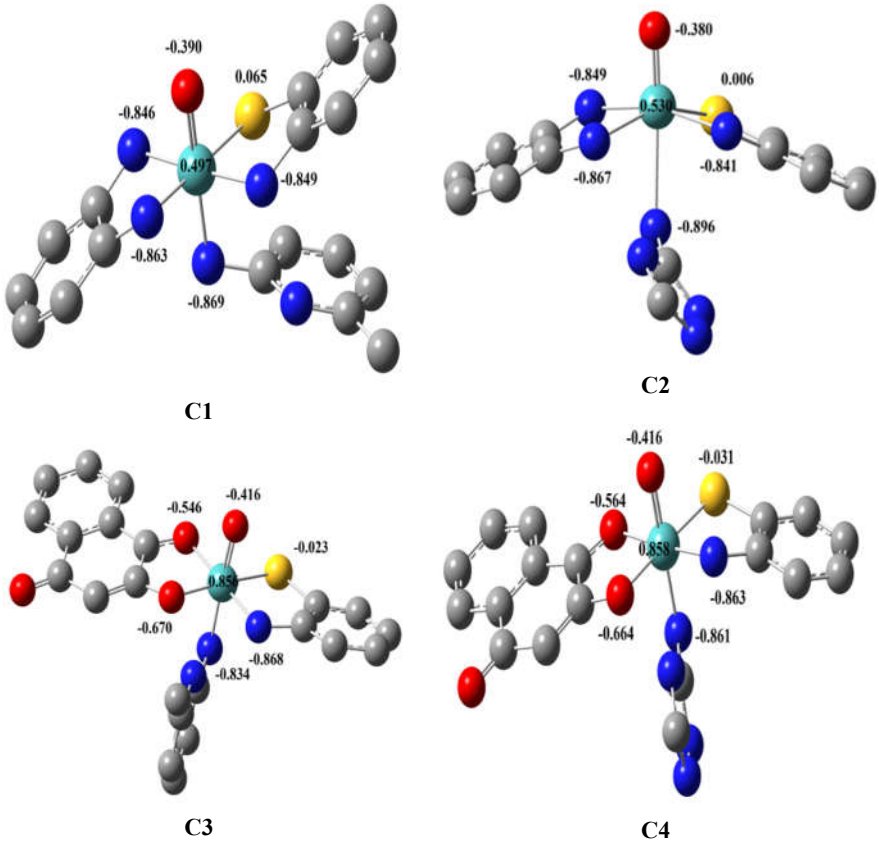

Figure 4. The suggested structures of the complexes with the natural bond order (NBO) charges.

Out of all the complexes, the C2 complex has the greatest polarity [32]. The energy range of the complexes are -1080.22 to -1392.55 a.u., while that of the ligands are -297.61 to -685.80 a.u. [32]. The HOMO, LUMO orbital energy, hardness (η), and ΔE values of the complexes are given in Table 3. The hardness (η) = ΔE/2, (HOMO-LUMO) = ΔE. The ΔE values, which range from 0.053 to 0.126, indicate that the complexes have easier transitions than the ligands based on the data acquired [32].

Antibacterial activity and MIC

The values of the inhibition zones and MIC against bacterial growth for the (ATP) ligand and the complexes are presented in Table 4. According to the results, the (ATP) ligand and the complexes showed moderate to good activity, whereas the (ATP) ligand has antibacterial activity with MIC values against the bacteria *S. aureus* (25 ppm), *E. coli* (50 ppm), *A. baumannii* (12.5 ppm), and *B. licheniformis* (12.5 ppm). The C1 complex didn't show inhibitory activity against *B. licheniformis*, *E. coli*, and *S. aureus* bacteria, while it inhibited *A. baumannii* at MIC values of 50 ppm. The C2 complex didn't show inhibitory activity against *E. coli*, *B. licheniformis*, and *S.*

aureus bacteria, while it inhibited *A. baumannii* at MIC values of 25 ppm. The C3 complex shows inhibitory activity with MIC values against the bacteria *S. aureus* (100 ppm), *E. coli* (50 ppm), and *A. baumannii* (12.5 ppm), but it did not show inhibitory activity against *B. licheniformis*. The C4 complex didn't show inhibitory activity against *S. aureus* and *B. licheniformis* bacteria, it has inhibitory activity with MIC values against E. coli (100 ppm) and *A. baumannii* (25 ppm). In general, the complexes antibacterial activity happens in this order: DMSO < ATP < C2 < C1 < C4 < C3. The fact that complexes had an expanded inhibition zone suggests that they were more lipophilic than the free ATP ligand, which aligns with Tweedy's complexes hypothesis [34].

Table 4. Antibacterial activities for ATP and its complexes.

Compound	Zone of inhibition (mm) and MIC								
	Conc. ppm	*S. aureus*	MIC	*E. coli*	MIC	*Acinetobacter Baumannii*	MIC	*Bacillus licheniformis*	MIC
ATP	100	22		-		18		25	+
	50	20		12	+	17		-	
	25	15	+	-		15		-	
	12.5	-		-		12	+	-	
C1	100	-		-		19		-	
	50	-		-		18		-	
	25	-		-		17		-	
	12.5	-		-		16	+	-	
C2	100	-		-		17		-	
	50	-		-		14	+	-	
	25	-		-		-		-	
	12.5	-		-		-		-	
C3	100	12	+	11		20		-	
	50	-		10	+	18		-	
	25	-		-		17		-	
	12.5	-		-		16	+	-	
C4	100	-		14	+	-		-	
	50	-		-		15		-	
	25	-		-		13	+	-	
	12.5	-		-		18		-	

Where: (-) No activity, (+) MIC.

Antioxidant activity of the complexes

The radical scavenging activity of gallic acid was determined by the free radical carrier DPPH (2,2-diphenyl-1-picryl-hydrazyl) when they interact with each other and is compared with the complexes where the radicals are scavenged by antioxidants after reduction, which can be measured by the decrease in absorbance at the wavelength 517 mm using an ultraviolet-visible device [35]. As gallic acid shows greater antioxidant activity at 60 min. The following ranking is for the antioxidant activity of the complexes: Gallic acid > C3 > C2 > C4 > C1 in 60 min, where the complexes showed the highest antioxidant activity by calculating the value of IC_{50}, which represents the half-maximum inhibitor for the tested samples, as in Figure 5 and also in Table 5. This shows that the high value comes to the C3 complex, followed by the C2 complex, then the C4 complex and C1 complex, with the highest value after the gallic acid, which is considered a substance compared to compounds because it is characterized by high oxidation.

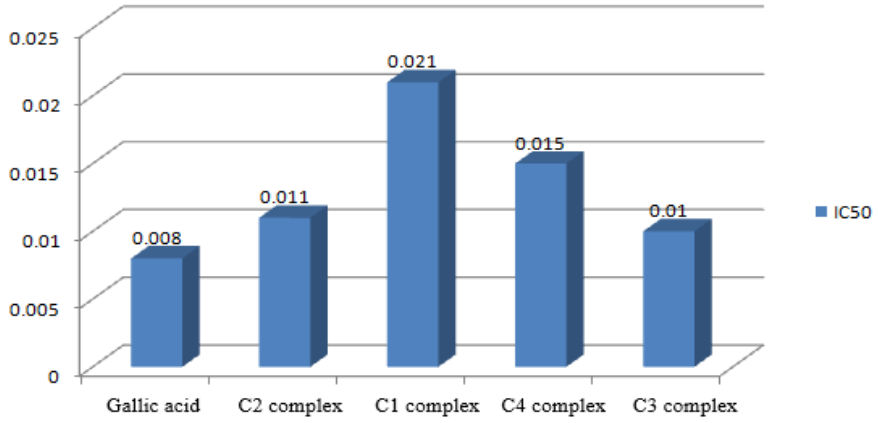

Figure 5. Variations of IC_{50} values for complexes.

Table 5. Radical scavenging activities, percentage inhibition and IC_{50} values.

Compound	Concentration	PI%	RSA%	IC_{50} mg/mL
Gallic acid	0.008	17.73	82.27	0.008
	0.004	44.69	55.31	
	0.002	59.35	40.65	
	0.001	67.16	32.84	
	0.0005	71.36	28.64	
C1	0.012	33.16	66.84	0.011
	0.006	49.85	50.15	
	0.003	58.45	41.55	
	0.0015	67.33	32.67	
C2	0.02	32.09	67.91	0.021
	0.01	42.07	57.93	
	0.005	51.39	48.61	
	0.0025	54.12	45.88	
C3	0.02	26.46	73.54	0.015
	0.01	42.71	57.29	
	0.005	52.22	47.78	
	0.0025	89.91	40.09	
C4	0.012	26.46	73.54	0.010
	0.006	41.65	58.35	
	0.003	52.05	47.95	
	0.0015	59.83	40.17	

CONCLUSION

The prepared complexes have an octahedral geometries. Based on the results of chemical and physical measurements, it is clear that the MoO(IV) complexes prepared from (ATP) with (DIAB) and (HNQ) ligands showed similarity in the quality of contact of the ligands with Mo(IV) ion, where behave as bidentate, while the (AMP) and (Atri) ligands coordinate with Mo(IV) ion as monodetantete ligand adduct through the nitrogen atoms that make up the amine group. Spectroscopic and DFT computations were used. According to the mass data, there is just one

nucleus in each complex. A study into magnetic susceptibility has shown that MoO(IV) complexes have a paramagnetic d^2 configuration. The molar electrical conductivity study showed that all complexes are non-electrolytes. The atomic absorption study and elemental analysis showed that the values of the products were identical to the calculated values. The peaks of the (d-d) metal transitions in complexes were revealed by the UV-Vis. measurements. The activity of the (ATP) ligand and the prepared complexes were examined against two Gram-negative and two Gram-positive bacteria. The complexes showed an expanded zone of inhibition, indicating that they were more lipophilic than the free (ATP) ligand. Finally, the antioxidant activity of the complexes was tested, and the results showed the following order: Gallic acid > C3 > C2 > C4 > C1 in 60 min.

REFERENCES

1. Nunes, P.; Correia, I.; Cavaco, I.; Marques, F.; Pinheiro, T.; Avecilla, F.; Pessoa, J.C. Therapeutic potential of vanadium complexes with 1, 10-phenanthroline ligands, quo vadis? The fate of complexes in cell media and cancer cells. *J. Inorg. Biochem.* **2021**, 217, 111350.
2. Li, H.; Wu, J.; Huang, X.; Lu, G.; Yang, J.; Lu, X.; Zhang, H. Rapid and reliable thickness identification of two-dimensional nanosheets using optical microscopy. *ACS Nano*. **2013**, 7, 10344-10353.
3. Odularu, A.T.; Ajibade, P.A.; Mbese, J.Z. Impact of molybdenum compounds as anticancer agents. *Bioinorg. Chem. Appl.* **2019**, 2019, 9.
4. Gisewhite, D.R.; Nagelski, A.L.; Cummins, D.C.; Yap, G.P.; Burgmayer, S.J. Modeling pyran formation in the molybdenum cofactor: Protonation of quinoxalyl–dithiolene promoting pyran cyclization. *Inorg. Chem.* **2019**, 58, 5134-5144.
5. Hernandez-Ruiz, R.; Sanz, R. Dichlorodioxomolybdenum(VI) complexes: Useful and readily available catalysts in organic synthesis. *Synthesis* **2018**, 50, 4019-4036.
6. Roy, S.; Lima, S.; Dhaka, S.; Maurya, M.R.; Acharyya, R.; Eagle, C.; Dinda, R. Synthesis, structural studies, and catalytic activity of a series of dioxidomolybdenum(VI)-thiosemicarbazone complexes. *Inorg. Chim. Acta* **2018**, 474, 134-143.
7. Ali, A.; Akram, W.; Liu, H.Y. Reactive cobalt–oxo complexes of tetrapyrrolic macrocycles and N-based ligand in oxidative transformation reactions. *Mol.* **2018**, 24, 78.
8. Fuior, A.; Cebotari, D.; Garbuz, O.; Calancea, S.; Gulea, A.; Floquet, S. Biological properties of a new class of $[Mo_2O_2S_2]$-based thiosemicarbazone coordination complexes. *Inorg. Chim. Acta* **2023**, 548, 121372.
9. Al-Ani, R.; Asaifi, M.; Kareem, H.; Alsaffar, A. Effect of different concentrations of molybdenum on dental enamel microhardness an in vitro study. *J. Med. Chem. Sci*. **2023**, 6, 1506-1516.
10. Berasaluce, I.; Cseh, K.; Roller, A.; Hejl, M.; Heffeter, P.; Berger, W.; Keppler, B.K. The first anticancer tris (pyrazolyl) borate molybdenum(IV) complexes: Tested in vitro and in vivo—A comparison of O, O-, S, O-, and N, N-chelate effects. *Chem. Eur. J.* **2020**, 26, 2211-2221.
11. Dhas, N.; Kudarha, R.; Garkal, A.; Ghate, V.; Sharma, S.; Panzade, P.; Mehta, T. Molybdenum-based hetero-nanocomposites for cancer therapy, diagnosis, and biosensing application: current advancement and future breakthroughs. *J. Control Release* **2021**, 330, 257-283.
12. Elsayed, S.A.; Noufal, A.M.; El-Hendawy, A.M. Synthesis, structural characterization, and antioxidant activity of some vanadium(IV), Mo(VI)/(IV), and Ru(II) complexes of pyridoxal Schiff base derivatives. *J. Mol. Struct.* **2017**, 1144, 120-128.
13. Spivack, B.; Dori, Z. Structural aspects of molybdenum(IV), molybdenum(V) and molybdenum(VI) complexes. *Coord. Chem. Rev*. **1975**, 17, 99-136.
14. Berasaluce, I.; Cseh, K.; Roller, A.; Hejl, M.; Heffeter, P.; Berger, W.; Keppler, B.K. The first anticancer tris (pyrazolyl) borate molybdenum(IV) complexes: Tested in vitro and in vivo-A comparison of O, O-, S, O-, and N, N-Chelate Effects. *Chem. Eur. J.* **2020**, 26, 2211-2221.

15. Nasibipour, M.; Safaei, E.; Wojtczak, A.; Jagličić, Z.; Galindo, A.; Masoumpour, M.S. A biradical oxo-molybdenum complex containing semiquinone and *o*-aminophenol benzoxazole-based ligands. *RSC Adv.* **2020**, 10, 40853-40866.
16. Kirakci, K.; Zelenka, J.; Rumlová, M.; Cvačka, J.; Ruml, T.; Lang, K. Cationic octahedral molybdenum cluster complexes functionalized with mitochondria-targeting ligands: Photodynamic anticancer and antibacterial activities. *Biomater. Sci*. **2019**, 7, 1386-1392.
17. Doğan, Ş.D.; Çetinkaya, Y.; Buran, S.; Yıldırım, S.Ö.; Butcher, R.J. Chemoselective synthesis, X-ray characterization, and DFT studies of new organic single crystal: S-(2-aminophenyl) cyclohexylcarbamothioate. *J. Mol. Struct.* **2020**, 1204, 127499.
18. Gök, Y.; Arlı, O.T.; Gök, H.Z.; Türkaslan, T. Rational synthesis of pH-responsive mesoporous organosilica nanoparticles functionalized with 2-aminothiophenol for controlled release of curcumin. *J. Porous Mater.* **2023**, 30, 1887-1896.
19. Rudnicka, M.; Ludynia, M.; Karcz, W. A comparison of the effects of 1, 4-naphthoquinone and 2-hydroxy-1, 4-naphthoquinone (lawsone) on indole-3-acetic acid (IAA)-induced growth of maize coleoptile cells. *Plant Growth Regul.* **2018**, 84, 107-122.
20. Mészáros, J.P.; Geisler, H.; Poljarević, J.M.; Roller, A.; Legina, M.S.; Hejl, M.; Enyedy, É. A. Naphthoquinones of natural origin: Aqueous chemistry and coordination to half-sandwich organometallic cations. *J. Organomet. Chem.* **2020**, 907, 121070.
21. de Freitas, P.P.; Ribeiro, R.C.B.; dos Santos Guimarães, I.; Moreira, C.S.; Rocha, D.R.; de Carvalho da Silva, F.; Gimba, E.R.P. (3, 3'-Methylene) bis-2-hydroxy-1, 4-naphthoquinones induce cytotoxicity against DU145 and PC3 cancer cells by inhibiting cell viability and promoting cell cycle arrest. *Mol. Biol. Rep.* **2021**, 48, 3253-3263.
22. Gehrke Jr, H.; Veal, J. Acetylacetonate complexes of molybdenum(V) and molybdenum(VI). *Inorg. Chim. Acta* **1969**, 3, 623-627.
23. Rodríguez-Melcón, C.; Alonso-Calleja, C.; García-Fernández, C.; Carballo, J.; Capita, R. Minimum inhibitory concentration (MIC) and minimum bactericidal concentration (MBC) for twelve antimicrobials (biocides and antibiotics) in eight strains of Listeria monocytogenes. *Biology* **2021**, 11, 46.
24. Mohamed, R.G.; Elantabli, F.M.; Aziz, A.A.A.; Moustafa, H.; El-Medani, S.M. Synthesis, characterization, NLO properties, antimicrobial, CT-DNA binding, and DFT modeling of Ni(II), Pd(II), Pt(II), Mo(IV), and Ru(I) complexes with NOS Schiff base. *J. Mol. Struct.* **2019**, 1176, 501-514.
25. Chang, Y.P.; Hector, A.L.; Levason, W.; Reid, G.; Whittam, J. Synthesis and properties of $MoCl_4$ complexes with thio-and seleno-ethers and their use for chemical vapor deposition of $MoSe_2$ and MoS_2 films. *Dalton Trans.* **2018**, 47, 2406-2414.
26. Alajrawy, O.I.; Almhmdi, A.A. Dioxomolybdenum(VI) and oxomolybdenum(IV) complexes with N, O, and S bidentate ligands, syntheses, spectral characterization, and DFT studies. *J. Mol. Struct.* **2022**, 1260, 132813.
23. Lee, C.; Weitao, Y.; Parr, R.G. Development of the Colle-Salvetti correlation- energy formula into a functional of the electron density. *Phys. Rev. B* **1988**, 37, 785-789.
24. Robinson R.Jr.; Abbasi K.K., Ariafard A.; Stranger R.; Yates B.F. Sulfur dioxide activation: a theoretical investigation into dual S═O bond cleavage by three-coordinate molybdenum(III) complexes. *Inorg. Chem.* **2015**, 54, 534-543.
25. Seghir, I.; Nebbache, N.; Meftah, Y.; Hachani, S.; Maou, S. DFT/TDDFT investigation on the electronic structure and spectroscopic properties of cis-dioxomolybdenum(VI) complexes. *Acta Chim. Slov*. **2019**, 66 3, 629-637.
26. Soliman, A.A.; Alajrawy, O.I.; Attabi, F.A.; Shaaban, M.R.; Linert, W. New formamidine ligands and their mixed ligand palladium(II) oxalate complexes: Synthesis, characterization, DFT calculations and in vitro cytotoxicity. *Spectrochim. Acta A Mol. Biomol. Spectrosc.* **2016**, 5, 358-69.

27. Soliman, A.A.; Attaby, F.A.; Alajrawy, O.I.; Majeed, S.R. Soluble ruthenium(II) with 3,4-diaminobenzoic acid complexes. *J. Therm. Anal. Calorim*. **2019**, 135, 2457-2473.
28. Soliman, A.A.; Sayed, A.M.; Alajrawy, O.I.; Linert, W. New palladium(II) formamidine complexes: Preparation, characterization, theoretical calculations, and cytotoxic activity. *J. Mol. Struct.* **2017**, 1137, 453-460.
29. Mohammed, B.A.; Ahmed, S.A.; Al-Healy, F. Design, characterizations, DFT, molecular docking and antibacterial studies of some complexes derived from 4-aminpantipyrine with glycine amino acid and ligand. *Bull. Chem. Soc. Ethiop*. **2024**, 38, 1609-1624.
29. Sabounchei, S.J.; Shahriary, P.; Salehzadeh, S.; Gholiee, Y.; Nematollahi, D.; Chehregani, A.; Amani, A.; Afsartala, Z. Pd(II) and Pd(IV) complexes with 5-methyl-5-(4-pyridyl)hydantoin: Synthesis, physicochemical, theoretical, and pharmacological investigation. *Spectrochim. Acta A Mol. Biomol. Spectrosc.* **2015**, 25, 1019-31.
30. Tweedy, B.G. Possible mechanism for reduction of elemental sulfur by monilinia fructicola. *Phytopathology* **1964**, 54, 910.
31. Al Zoubi, W.; Al-Hamdani, A.A.S.; Duraid Ahmed, S.; Basheer, H.M.; Al-Luhaibi, R.S.A.; Dib, A.; Ko, Y.G. Synthesis, characterization, and antioxidant activities of imine compounds. *J. Phys. Org. Chem*. **2019**, 32, 3916.
32. Taher, S.R.; Hamad, W.M. Synthesis, characterization, density functional theory (DFT) analysis, and mesomorphic study of new thiazole derivative. *Bull. Chem. Soc. Ethiop*. **2024**, 38, 1827-1842.